Journal of Controlled Release 196 (2014) 363–369

Contents lists available at ScienceDirect

Journal of Controlled Release

journal homepage: www.elsevier.com/locate/jconrel

Material-mediated proangiogenic factor release pattern modulates quality of regenerated blood vessels

Max H. Rich [a,b], Min Kyung Lee [a,b], Kwanghyun Baek [c], Jae Hyun Jeong [d], Dong Hyun Kim [e], Larry J. Millet [f,g], Rashid Bashir [f,g], Hyunjoon Kong [a,b,g,*]

[a] Department of Chemical and Biomolecular Engineering, University of Illinois at Urbana-Champaign, Urbana, IL 61801, USA
[b] Institute for Genomic Biology, University of Illinois at Urbana-Champaign, Urbana, IL 61801, USA
[c] Department of Material Science & Engineering, University of Illinois at Urbana-Champaign, Urbana, IL 61801, USA
[d] Department of Chemical Engineering, Soongsil University, Seoul 145-743, South Korea
[e] Korea Institute of Industrial Technology, Ansan 426-910, South Korea
[f] Department of Bioengineering, University of Illinois at Urbana-Champaign, Urbana, IL 61802, USA
[g] Electrical and Computer Engineering, University of Illinois at Urbana-Champaign, Urbana, IL 61802, USA

ARTICLE INFO

Article history:
Received 3 July 2014
Accepted 16 October 2014
Available online 24 October 2014

Keywords:
Angiogenesis
Hydrogel
Ink-jet printing
Vascular endothelial growth factor

ABSTRACT

Hydrogels designed to sustainably release bioactive molecules are extensively used to enhance tissue repair and regenerative therapies. Along this line, numerous efforts are made to control the molecular release rate and amount. In contrast, few efforts are made to control the molecular release pattern, and, subsequently, modulate the spatial organization of newly forming tissues, including blood vessels. Therefore, using a hydrogel printed to release vascular endothelial growth factor (VEGF) into a pre-defined pattern, this study demonstrates that spatial distribution of VEGF is important in guiding growth direction of new blood vessels, and also in retaining the structural integrity of pre-existing vasculature. Guided by a computational model, we fabricated a patch composed of micro-sized VEGF-releasing poly(ethylene glycol) diacrylate (PEGDA) hydrogel cylinders using an ink-jet printer. Interestingly, hydrogel printed with computationally optimized spacing created anisotropically aligned vasculature exclusively when the printed gel pattern was placed parallel to pre-existing blood vessels. In contrast, vascular sprouting from placing the printed gel pattern perpendicular to pre-existing vessels resulted in deformation and structural disintegration of the original vasculature. We envision that this study will be useful to better understand angiogenesis-modulated neovascularization and further improve the treatment quality for various wounds and tissue defects.

© 2014 Elsevier B.V. All rights reserved.

1. Introduction

Efforts to regenerate functional tissue have emerged as a promising strategy to prepare biomedical tools invaluable to better understand development, homeostasis, and pathogenesis [1–6]. These tools enable the further enhancement of treatments for acute and chronic diseases as well as tissue defects [1,7]. One of the main approaches to accomplish this goal is to deliver cell-instructive bioactive molecules, such as growth factors and cytokines, in order to activate or deactivate cellular phenotypic activities involved in tissue development and homeostasis [8,9]. To sustain bioactivity of these molecules, various biomaterials processed in the form of particles, microporous matrices, and hydrogels, are being assembled as molecular carriers [10–14]. Extensive efforts were made to control the release rate of these bioactive molecules from biomaterials, because control of the release rate is important for stimulation of cellular activities during the desired time period [2,11,15,16].

In contrast, few efforts were made to tailor the spatial distribution of bioactive molecules, despite its potential importance in guiding growth direction and spacing of newly forming tissues [17]. For instance, an approach to rebuild microvascular networks, termed as revascularization, is performed by activating capillary sprouting from pre-existing vasculature. Success in this approach greatly relies on the ability to control spatial organization of vasculature, because it is not only important in attaining uniform tissue perfusion, but also retaining the structural integrity of pre-existing blood vessels [1,17,18]. If the spacing between new vasculature is too narrow (i.e., smaller than 300 μm), then there is a high likelihood of inflammation [19,20]. In contrast, if the spacing between vessels is too large, then the vasculature fails to sufficiently perfuse tissues of interest. In addition, new vasculature sprouting from pre-existing blood vessels may exert tensile forces and affect structural integrity of the original vasculature [21,22].

* Corresponding author at: Department of Chemical and Biomolecular Engineering, University of Illinois at Urbana-Champaign, Urbana, IL 61801, USA. Tel.: +1 217 244 9214; fax: +1 217 333 5052.
E-mail address: hjkong06@illinois.edu (H. Kong).

http://dx.doi.org/10.1016/j.jconrel.2014.10.020
0168-3659/© 2014 Elsevier B.V. All rights reserved.

This study demonstrates that the spatial distribution of pro-angiogenic growth factor such as VEGF is not only important in increasing the density of new blood vessels but also retain structural integrity of pre-existing vasculature. A patch constituting of micro-sized, vascular endothelial growth factor (VEGF)-releasing poly(ethylene glycol) diacrylate (PEGDA) hydrogel cylinders was constructed using an ink-jet printer. Guided by diffusion-based computational simulation, the hydrogel cylinders were built to present spacing large enough to attain local increases in growth factor concentration. The resulting patch was implanted on a chicken chorioallantoic membrane to examine vascularization under the patch. Specifically, the hydrogel cylinders were placed in parallel with pre-existing vessels or perpendicular to them, in order to examine whether the growth direction of capillary sprouts affects the structural integrity of pre-existing blood vessels (Scheme 1). Overall, the results of this study will greatly serve to improve the quality of revascularization therapies and also better understand developmental and pathological vascularization processes.

2. Experimental section

2.1. Materials

Poly(ethylene glycol) diacrylate (PEGDA) (M_n ~700) and Pluronic® F-127 were purchased from Sigma Aldrich. Human recombinant VEGF 165 and human Duo VEGF enzyme-linked immunosorbent assay (ELISA) kits were purchased from R&D Systems. Phosphate buffered saline (PBS) without magnesium and calcium and Penicillin/Streptomycin (P/S, 10,000 U/mL and 10,000 mg/mL) was purchased from Cellgro. Fertilized chicken eggs (Hy-Line W-36) were obtained from the University of Illinois Poultry Farm (Urbana, IL). Rhodamine B-Dextran (10,000 MW) was purchased from Invitrogen. Circular 18 mm cover glass no. 1 was purchased from VWR. Dimatix materials printer cartridges (DMC-11610) were purchased from Fujifilm. 3-(Trimethoxysilyl)propyl methacrylate was purchased from Sigma Aldrich. 200 proof ethyl alcohol (2701) came from Decon labs. The photoinitiator, 1-[4-(2-hydroxy-ethoxy)-phenyl]-2-hydroxy-2-methyl-1-propane-1-one (Irgacure 2959) was purchased from Ciba. Dimethyl sulfoxide (DMSO) was purchased from Fisher Scientific.

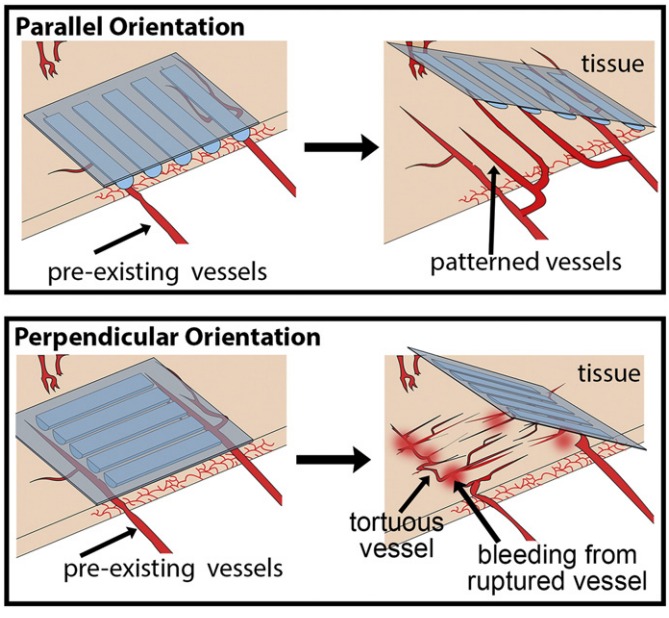

Scheme 1. Schematic of the dependence of implant orientation on neovessel quality. The schematic depicts that alignment of VEGF-releasing hydrogel bars in the patch parallel to pre-existing vessels results in new vessels with similar, anisotropic alignments (top). In contrast, aligning VEGF-releasing hydrogel bars perpendicular to pre-existing vessels causes the deformation of pre-existing vessels. The vascular deformation results in tortuosity of and blood-leaking from vessels (bottom).

2.2. Characterization of hydrogel properties

Hydrogel stiffness was quantified by measuring the compressive elastic modulus (E). After incubating the gel disks with 1 mm-thickness and 1 cm-diameter in PBS for 48 h, gel disks were uniaxially compressed at a rate of 1 mm per minute using a mechanical testing system (MTS Insight). The slope of the stress versus strain curve was used to calculate E from the first 10% of strain. The swelling ratio (Q_m) was calculated by measuring the ratio of wet mass to dry mass of the gels. The wet mass of the gel was measured after incubating the gel in PBS for 48 h.

2.3. Formulation of hydrogel-forming solution

The ink was prepared by mixing 4 vol.% PEGDA solution and 10 vol.% Pluronic solution at varied ratios. These two solutions were diluted with deionized water to attain the desired concentrations in the mixture. Additionally, 40 μL of Irgacure 2959 was added per mL of PEGDA ink. For vascularization study, 1 μg of VEGF was added per mL of PEGDA ink.

2.4. Measurement of viscosity of hydrogel-forming solution

The viscosity was measured using a viscometer (Brookfield DV II+ pro). A 750 μL PEGDA ink was loaded between a cone with 48 mm diameter and a plate. The shear rate was fixed at 20 rpm and the resulting stress was measured by the viscometer. The viscosity, a ratio between shear stress and shear rate, was recorded by a computer.

2.5. Measurement of surface tension of gel-forming solution

A drop tensiometer (Attension Theta Lite) was used to measure the surface tension of the PEGDA ink. Approximately 1 mL PEGDA ink was loaded into a syringe, inverted, and then the needle was centered and focused in the frame of tensiometer's camera. Next, the biggest hanging drop possible was formed on the tip of the needle. A picture was then taken of the hanging drop. The Attension Theta computer software was then used to quantify the radius of drop curvature at apex (R_0), the difference in density between the fluid and air ($\Delta\rho$), the gravitational constant (g), the shape factor (β), and the Young–Laplace equation, Eq. (1),

$$\gamma = \Delta\rho g \frac{R_0^2}{\beta} \tag{1}$$

in order to determine the surface tension of the fluid.

2.6. Printing of PEGDA ink and subsequent gel assembly

The gel-forming PEGDA ink was printed on circular cover glass with 18 mm diameter. Prior to the printing, the glass was exposed to plasma for 5 min, and subsequently immersed in a 2% 3-(trimethoxysilyl) propyl methacrylate solution diluted in 200 proof ethyl alcohol for 10 min. Then, the coverslips were baked at 110 °C on a hot plate until dry and rinsed with 200 proof ethyl alcohol. For imaging of the resulting gel, PEGDA ink was mixed with rhodamine B-Dextran (MW ~10,000 g/mol) at a concentration of 0.5 vol.%.

Three coverslips were placed on a microscope slide, 500 μm (thickness) × 75 mm (length) × 25 mm (width), held down by 5 μL of deionized water. 1 mL of the PEGDA ink was degassed and filtered through a 0.22 μm filter for sterilization. Then, the ink was loaded into the ink-jet cartridge (Dimatix type 11610). Droplet ejection condition was optimized using the Dimatix Drop Manager software as described

previously [23]. Voltage applied to expel the ink through the jets was set to −30 mV. Substrate height was set to 600 μm and temperature was kept constant at room temperature (25 °C). Patterns for printing were programmed through the Drop Manager software as described previously [23]. Following completion of printing, the slides were exposed to UV light at 254 nm for 10 min to activate the cross-linking reaction to form a gel. The printed gel constructs were incubated in PBS supplemented with 2 vol.% penicillin/streptomycin until use. The resulting printed gel construct was imaged using a fluorescent microscope (Olympus BX51 Upright Fluorescence Micro).

2.7. Analysis of VEGF release

The VEGF release from the printed hydrogel over 10 days was characterized by measuring the VEGF concentration in incubation media using the human VEGF ELISA kit per the manufacturer's protocol. Briefly, a 96 well plate was coated with capture antibody overnight. Any antibody that failed to adhere to the plate was then washed away and the plates were blocked with bovine serum albumin for 1 h. The plates were then washed and incubated with the samples and standards for 2 h followed by another wash step. The plates were then incubated with detection antibody (2 h) followed by washing and further incubated with streptavidin-horseradish-peroxidase (20 min). Following another washing step, the samples were incubated with a 1:1 mixture of hydrogen peroxide (color reagent A) and tetramethylbenzidine (color reagent B), called substrate solution. The colorimetric reaction was stopped with 2 N sulfuric acid. Finally, the absorbance of the plate at 570 nm was subtracted from the reading at 450 nm to determine the absorbance of the samples and standards. The PEGDA hydrogel disk formed by exposing bulk PEGDA solution to UV light was prepared for a control experiment. A standard curve was developed by measuring the absorbance of solutions with known VEGF concentrations and then used to determine the concentrations released at different time points from the hydrogels.

2.8. Simulation

3D finite element models for hydrogel constructs and chorioallantoic membrane (CAM) were created using Comsol Multiphysics 4.1. It was assumed that the protein release from the hydrogel was governed by the Fick's first law of diffusion. Two hydrogels used in the model include (1) the linear arrays of half-cylinders with 160 μm-diameter and 120 μm-spacing, and (2) the linear arrays of half-cylinders with 160 μm-diameter and 350 μm-spacing. The concentration of VEGF in the hydrogel was kept constant at 5×10^5 mol/m^3. The CAM membrane was modeled as being 300 μm thick with a constant concentration of zero at the lower boundary of the model. This constant zero concentration acted as a sink, thereby consuming the VEGF once it reached the bottom surface of the model. It was assumed that hydrogel arrays were embedded in the top of the membrane. In this numerical analysis, diffusion coefficients of drug in media, tissue, and hydrogel were approximated to be 100 μm^2/s, 1 μm^2/s, and 0.02 μm^2/s, respectively [24]. The units used for all simulations were meters, seconds, and kilograms.

2.9. In vivo chorioallantoic membrane (CAM) assay for neovascularization

Fertilized eggs were incubated horizontally at 37 °C and 65% humidity for 7 days. A window was then made in the shell big enough to insert the coverslips, while being careful to avoid shell fragments falling onto the membrane. Then, the window was covered with scotch tape and the egg was incubated overnight at 37 °C to ensure the egg's viability after making the window. On the following day, hydrogel samples were implanted onto the CAMs of the embryos and incubated at 37 °C for 7 days. Pictures of the CAM were taken after the initial implantation and after 7 days to capture neovascularization using a Leica S6E stereomicroscope linked with a Leica D-Lux E Camera. The entire CAM experiment was performed under sterile conditions.

On the seventh day following implantation, the CAM was fixed using a 4% neutral buffered formalin solution at 4 °C for 2 h. The CAM around the coverslip was cut out using suture scissors and imaged using the stereoscope. Finally, the fixed CAM was prepared for paraffin embedding, sectioning, and stained for α-smooth muscle actin (αSMA) using standard histological procedures. Images of the αSMA stained tissue were used to quantify the average number of blood vessels including ones not visible through top-view digital images of the explanted tissue. The vessel diameter and the ratio of blood vessel to total tissue area were quantified using ImageJ.

2.10. Statistical analysis

Four samples were analyzed per condition. One-way analysis of variance (ANOVA) was used to determine the statistical significance of data. Tukey's post-hoc tests were applied to all the pairwise differences between means. Data was considered significant for p values < 0.05.

3. Results and discussion

Success in controlling spatial distribution of exogenous VEGF greatly depends on the ability to print a VEGF-releasing gel in a pre-defined micropattern. It is well agreed that viscosity and surface tension of a pre-gel solution are critical to print it in a desired pattern [23], because they influence solution flux during jetting and also retention of the printed pattern on the substrate. For example, the pre-gel solution with too high viscosity or surface tension does not steadily flow out of a jet nozzle. Conversely, the solution with too low viscosity and surface tension cannot retain the printed pattern. In this study, we tailored the viscosity and surface tension of the gel-forming PEGDA solution using Pluronic with a molecular weight of 12,700 Da (Fig. 1A).

At a given PEGDA concentration, increasing the Pluronic concentration resulted in an exponential increase of the viscosity of pre-gel solutions (Figs. S1A & S2). For 4 and 6 vol.% PEGDA solutions, increasing the Pluronic concentration from 0 to 10% resulted in an 8-fold increase of the solution viscosity. Separately, the surface tension of the PEGDA solution was decreased from 55 to 44 mN/m by adding 2 vol.% Pluronic, at given PEGDA concentrations. Further increase of the Pluronic concentration to 6 vol.% made minimal changes to the surface tension (Figs. S1B & S2). These results address that Pluronic controls the viscosity of pre-gel PEGDA solution over a broad range, while keeping the surface tension at a constant level of 40 mN/m.

We further printed pre-gel PEGDA–Pluronic solutions with varying viscosity and surface tension on a glass substrate using an ink-jet printer, in order to validate the important roles of these two properties in the quality of gel printing (Fig. 1A). The 4 vol.% PEGDA + 0 vol.% Pluronic solution with viscosity of 2 cP and surface tension of 55 mN/m (Fig. 1A-I) and the 6 vol.% PEGDA + 10 vol.% Pluronic solutions with viscosity of 10 cP and surface tension of 40 mN/m (Fig. 1A-II) were bled from the originally printed area and could not maintain the printed pattern on the substrate. The 10 vol.% PEGDA + 10 vol.% Pluronic solution with viscosity of 16 cP and surface tension of 40 mN/m was printed with frequent interruption, due to unsteady flow of pre-gel solution during jetting (Fig. 1A-IV). In contrast, the 4 vol.% PEGDA + 10 vol.% Pluronic solution with viscosity of 12 cP and surface tension of 40 mN/m was printed in a desired form without any solution run or discontinued defects (Fig. 1A-III). Overall, this study demonstrated that viscosity and surface tension of the pre-gel solution for optimal printing should be 12 cP and 40 mN/m, respectively.

The pre-gel solution with viscosity of 12 cP and surface tension of 40 mN/m allowed us to build a gel with varied shape and spacing via sequential printing of the pre-gelled solution on a methacrylate-functionalized glass substrate followed by exposure to UV light (Fig. 1B). For instance, a hydrogel was printed in forms of multiple linear

half-cylinders or cross-patterned half-cylinders with controlled width and spacing (Fig. 1C). Hydrogel circles with 50–172 μm diameters were also printed on a substrate while varying spacings over a broad range. The printed hydrogel remained adhered to the glass substrate during incubation in phosphate buffer saline (PBS). The hydrogel printed on the unmodified glass was separated from the glass during incubation in PBS. Pluronic made minimal effects on both elastic modulus and swelling ratio of the resulting gel (Fig. S4).

These printed PEGDA hydrogels were further functionalized by mixing VEGF with the pre-gel solution and activating the cross-linking reaction of PEGDA. The PEGDA hydrogel sustainably released VEGF over 10 days, independent of its printed pattern (Fig. S3). The release pattern from the patch consisting of multiple gel cylinders well fitted to a model with an approximation of Fick's second law of diffusion,

$$\frac{M_t}{M_\infty} = 4\left(\frac{Dt}{\pi R^2}\right)^{\frac{3}{2}} - \frac{Dt}{R^2} \tag{2}$$

where M_t is the concentration of VEGF at time t, M_∞ is the concentration released after infinite time, and R is the radius of the printed half-cylinder. According to the calculation, the D of the VEGF in the printed PEGDA hydrogel was 2×10^{-14} m^2/s, independent of the spacing between printed hydrogel half-cylinders.

We further computationally estimated the distance between printed hydrogel above which VEGF concentrations would be locally increased within tissue in contact with the gel cylinders. According to the simulation result conducted using finite element modeling, a hydrogel printed with spacing of 120 μm would result in a local increase in VEGF concentration around the gel bars, similar to a bulk hydrogel (Fig. 2A & B). In contrast, increasing the gel spacing to 350 μm would generate a local increase of the VEGF concentration around the printed gel cylinders in implanted tissue (Fig. 2C). These results implicate that hydrogel bars larger than 350 μm-spacing are able to build vasculature following the printed gel pattern, while those with 120 μm-spacing would fail to control vascular growth direction and spacing.

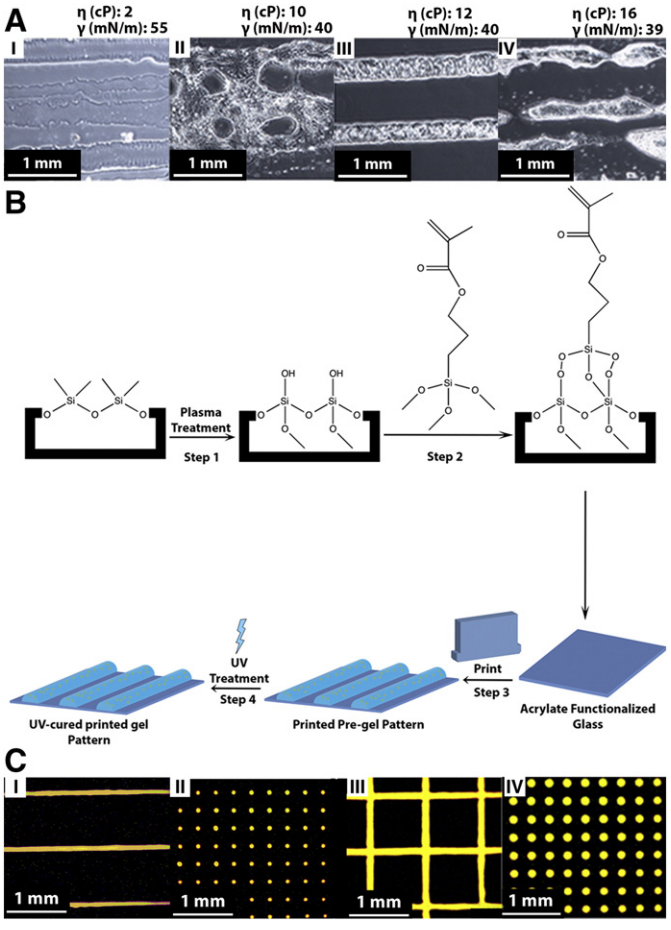

Fig. 1. Properties of inkjet-printed hydrogel. (A) Images of inkjet-printed pre-gel solution showing the dependence of print quality on viscosity and surface tension. (B) Scheme of preparing the micropatterned gel via silanization of a substrate, printing of pre-gel solution, and photo-induced cross-linking reaction for gel-formation. (C) At the optimal surface tension and viscosity (40 mN/m and 11.80 cP), it was possible to print the ink in a variety of patterns demonstrated in the fluorescence images. Fluorescence images were taken by dissolving 0.01% rhodamine into the pre-gel solution.

To validate the simulation result, the VEGF-encapsulated PEGDA hydrogel was printed in a form of multiple, line-shaped bars with 160 μm width and 350 μm spacing, and implanted on the chicken chorioallantoic membrane (CAM) (Fig. 3A). Hydrogels were printed with a width of 160 μm, as that was the smallest printable width with our formulated pre-gel solutions. In this study, the printed gel was placed between two pre-existing vessels with the bar direction parallel to the pre-existing vessels (Fig. 3B). Very interestingly, throughout implantation over 7 days, multiple, anisotropically aligned blood vessels with an average 300 μm-spacing were created between two pre-existing vessels covered with hydrogel cylinders with 350 μm-spacing (Fig. 3C3-II). These vessels were connected to two blood vessels branched out of the pre-existing vasculature. Therefore, the direction of new vessels was in parallel with pre-existing ones. In contrast, control conditions including CAMs implanted with a bulk hydrogel and hydrogel bars with 120 μm spacing showed new vessel growth under the implant, but without any discrete vascular pattern (Fig. 3C1-II & C2-II). Additional control experiments with no implant, implant of bulk gels containing no VEGF, and implant of VEGF-free hydrogel bars with 120 μm and 350 μm spacings demonstrated that very few blood vessels formed in these conditions (Figs. S5, 3D, and E).

According to histological analysis of mature blood vessels marked by α-smooth muscle actin, increasing the spacing between hydrogel bars led to a larger vascular density of the implanted tissue, although the mass of VEGF loaded in the gel was equivalent between conditions (Fig. 3C3, D & E). Specifically, hydrogel bars with 350 μm-spacing created 3 and 1.5-times larger number of blood vessels than the bulk hydrogel without any spacing and that with 120 μm-spacing, respectively. In particular, the hydrogel bars with 350 μm-spacing significantly increased the number of vessels with 40 to 140 μm-diameter, compared to those with 120 μm-spacing. However, for blood vessels with diameters larger than 200 μm, the number of blood vessels was slightly higher with the hydrogel printed with 120 μm spacing than that printed with 350 μm spacing (Fig. 3D & E).

Additionally, the alignment of hydrogel bars with pre-existing blood vessels played very important roles in stimulating sprouting of capillaries while retaining structural integrity of pre-existing vessels (Fig. 4A). Hydrogel bars placed perpendicular to pre-existing vessels stimulated sprouting of multiple blood vessels, most of which were aligned normal to the direction of pre-existing vessels (Fig. 4B). These multiple blood vessels greatly deformed the original blood vessels into a tortuous form. Additionally, some pre-existing vasculature displayed the rupture, thus causing bleeding into tissue (Fig. 4C). Furthermore, according to hematoxylin and eosin (H&E)-stained histological images, a larger number of immune cells were mobilized in CAM implanted with hydrogel bars printed perpendicular to pre-existing vessels than CAM implanted with hydrogel bars aligned with pre-existing ones. Subsequently, CAM became thicker when the printed gel bars were aligned perpendicular to pre-existing ones.

Overall, this study demonstrates a unique method to formulate a hydrogel that can be printed in a desired micropattern and used to control spatial distribution of molecular distribution. We interpret that Pluronic copolymers introduced into PEGDA solution self-aggregate in the pre-gelled solution, thus serving to increase the viscosity of the solution proportional to its concentration. These self-aggregated Pluronic molecules also reduce surface tension of the pre-gelled solution, because of the interaction with the hydrophilic portions of the polymer. It is suggested

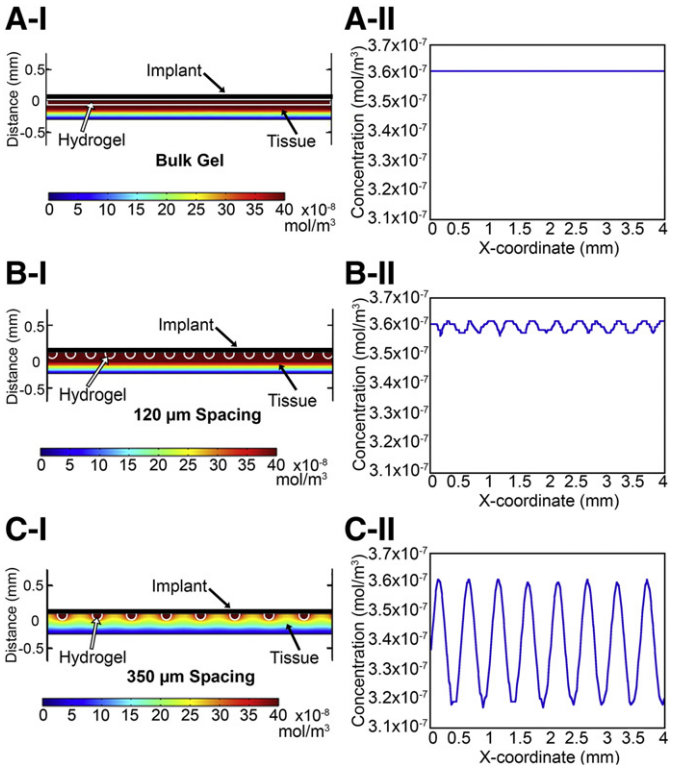

Fig. 2. Computational simulation of VEGF distribution in tissue implanted with a bulk gel (A), inkjet-printed gel bars with a spacing of 120 μm (B), and inkjet-printed gel bars with a spacing of 350 μm (C). Diameter of the hydrogel was kept constant at 18 mm. In (A)–(C), (I) displays two dimensional distribution of VEGF within tissues implanted with materials and (II) does one dimensional VEGF concentration within tissues. In (I), number on the Y-axis represents distance from tissue implanted with hydrogels.

that the Pluronics self-organize to present hydrophobic portions at the air–water interface, limiting the interactions between water molecules and, thereby, reducing the surface tension [25]. The surface tension could not be further reduced past 40 mN/m, though, likely because the air–water interface is fully saturated with the hydrophobic portions of the Pluronics. This approach to control viscosity and surface tension of hydrogel-forming solution for a printing using an ink-jet printer is distinctive from previous approaches that printed various cell adhesion molecules on a hard substrate for cell culture, assay, biosensors, and biochips [26].

Another highlight of this study is that a drug-releasing hydrogel could be printed into a pattern that can control growth direction and spacing of blood vessels, guided by the computational modeling. The vascular patterning attained by the hydrogel bars with proper spacing should be attributed to the local and temporal increase of VEGF concentration in tissue area in direct contact with the printed gel, according to the diffusion-based modeling. It is suggested that endothelial precursor cells in pre-existing blood vessels develop endothelial sprouts following such locally increased VEGF patterns and finally form the vasculature with the equivalent spacing as the printed gels. Such vascular patterning was advantageous to increase vascular density within targeted tissue, thus potentially enhancing perfusion. It is likely that the effects of vascular patterning would be further improved by increasing VEGF loading in the printed gel, incorporating supplemental proangiogenic factors such as platelet-derived growth factor (PDGF) [27], and conjugating growth factor-binding peptides to the gel-forming polymer [28]. Additionally, in future studies using a mouse model implanted with various printed hydrogel patches, the vascular density including capillaries will be examined.

This study further demonstrated that alignment of newly formed blood vessels with pre-existing blood vessels is important in stimulating

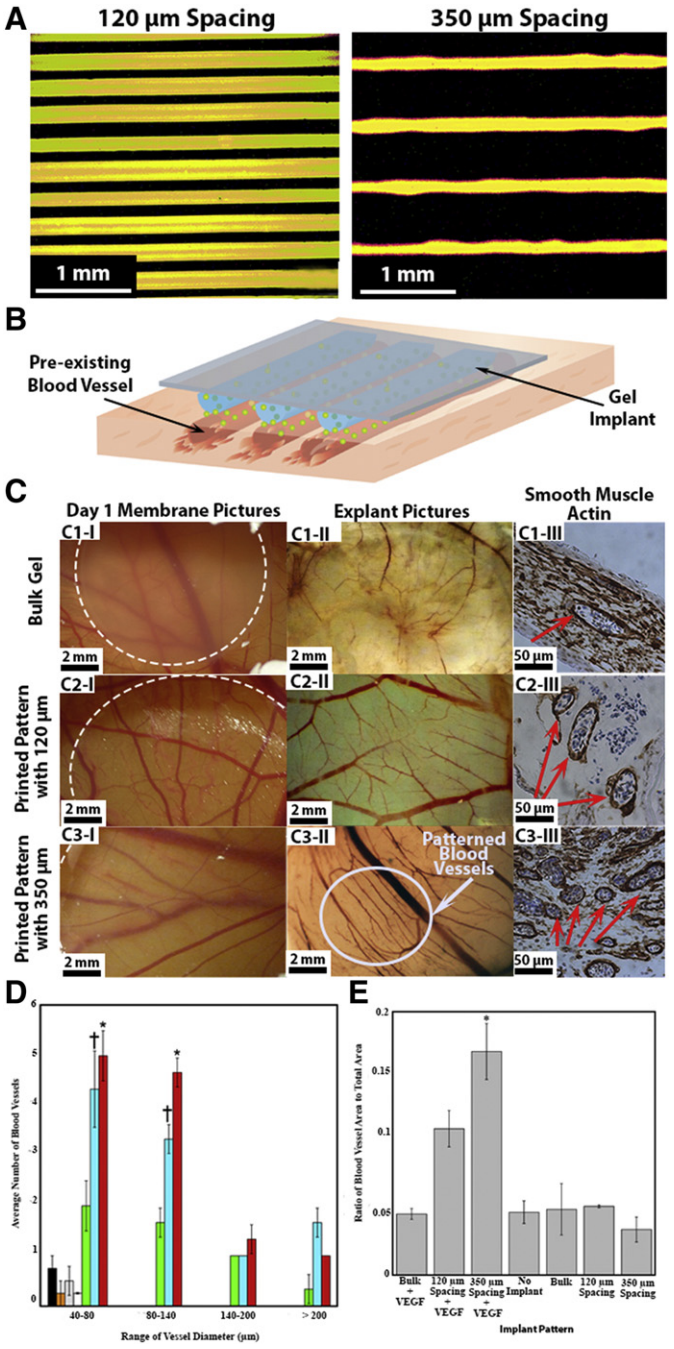

Fig. 3. *In vivo* CAM analysis of effects of hydrogel bar spacing on vascularization. (A) Fluorescence images of hydrogel printed with 120 μm and 350 μm spacings. (B) Schematic describing hydrogel bars implanted in parallel with original arteries. (C) CAM implanted with a hydrogel disk (C-1), CAM implanted with an inkjet printed hydrogel with a bar spacing of 120 μm (C-2), and CAM implanted with an inkjet printed hydrogel with a bar spacing of 350 μm (C-3). Images on the first column were captured on the first day of implantation. The dotted lines outline the implant. Those on the 2nd column were captured seven days after implantation. Images on the 3rd column are cross-sectional images of CAM stained for α-smooth muscle actin. The red arrows in the 3rd column point to mature blood vessels surrounded by smooth muscle actin layer. (D) Quantitative analysis of the number of blood vessels at given diameter ranges in CAM implanted with no implant (black), a bulk hydrogel disk (orange), a bulk hydrogel disk with VEGF (green), inkjet-printed hydrogel bars printed with a spacing of 120 μm (gray) and 350 μm (white), and inkjet-printed hydrogel bars loaded with VEGF and a spacing of 120 μm (blue) and 350 μm (red). (E) Quantitative analysis of areal fraction of total blood vessels in CAM. In (D) & (E), * indicates statistical significance of values between VEGF-loading hydrogel bars printed with 350 μm spacing and other conditions ($p < 0.05$, n = 4). In (D), † indicates statistical significance of values between VEGF-loading hydrogel bars printed with 120 μm spacing and other conditions ($p < 0.05$, n = 4).

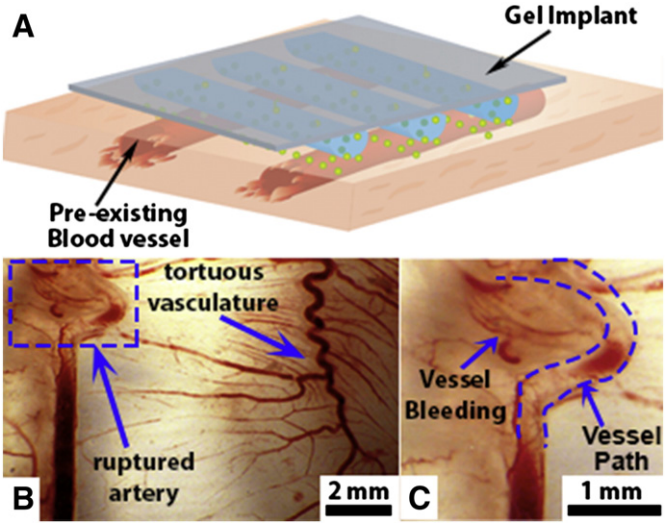

Fig. 4. Deformation of original vasculature due to placement of hydrogel bars perpendicular to the pre-existing arteries. (A) Schematic describing hydrogel bars implanted perpendicular to original arteries. (B) Images of vasculature in CAM implanted with the inkjet-printed gel with a bar spacing of 350 μm. (C) Magnified view of the ruptured artery shown in the box in (B).

functional vasculature without encountering any negative side-effects. We interpret that hydrogel cylinders placed in parallel with pre-existing arteries stimulate two endothelial sprouts from pre-existing ones, which are perpendicular to each other. Then, multiple blood vessels should be sprouted from two endothelial sprouts, following the pattern of printed gel bars. In contrast, the hydrogel cylinders placed perpendicular to pre-existing arteries stimulated multiple blood vessels directly from pre-existing ones, thus implementing unidirectional tensile forces on vasculature. Such mechanical force should deform pre-existing arteries, thus deforming vasculature into a tortuous pattern [29]. Subsequently, external force likely weakened endothelial junction, thus resulting in vascular leakage. Such deformed, leaky vasculature activates recruitment and extravasation of leukocytes and subsequently induces pro-inflammation [30]. We suggest that this result improves the understanding on the mechanism by which VEGF-based revascularization therapies are often plagued by undesirable pro-inflammation [31–34], as well as limited increase of the vascular density [35–40].

4. Conclusion

Overall, this study presents an advanced method of printing a PEGDA hydrogel that can create vasculature with a pre-defined micropattern. The viscosity and surface tension of the gel-forming PEGDA solution were tuned to values appropriate for the ink-jet printing using Pluronic. The sequential printing of the mixture of PEGDA solution and VEGF into desired micro-pattern and photo cross-linking reaction resulted in a hydrogel which sustainably releases VEGF via diffusion. According to the diffusion-based simulation, the hydrogel bars printed to have a spacing large enough to locally increase VEGF concentration in the implanted tissue successfully created vasculature which followed the micropattern of the hydrogel bars. The alignment between hydrogel bars and pre-existing vasculature was also important in creating patterned vasculature without disturbing structural integration of the pre-existing ones. We propose that the hydrogel assembled in this study should greatly assist one to better understand vascular development, regeneration, and pathogenesis. Additionally, the gel would be readily used to treat ischemic tissues and tissue defects due to its capability to increase vascular density, which will be examined in near future studies [41,42].

Acknowledgments

This work was supported by National Science Foundation (CAREER: DMR-0847253 to H.K., STC-EBICS grant CBET-0939511 to H.K & R.B.), US Army Telemedicine & Advanced Technology Research Center (W81XWH-08-1-0701 to H.K. & R.B.), Korea Institute of Industrial Technology (JE140004) (to H.K), Center for Advanced Study, University of Illinois at Urbana-Champaign (to H.K.), and University of Illinois Dow Chemical Company Fellowship (to M.R).

Appendix A. Supplementary data

Supplementary data to this article can be found online at http://dx.doi.org/10.1016/j.jconrel.2014.10.020.

References

[1] R.R. Chen, E.A. Silva, W.W. Yuen, D.J. Mooney, Pharm. Res. 24 (2) (2006) 258–264, http://dx.doi.org/10.1007/s11095-006-9173-4.
[2] R.J. DeVolder, H. Bae, J. Lee, H. Kong, Adv. Mater. 23 (28) (2011) 3139–3143, http://dx.doi.org/10.1002/adma.201100823.
[3] A.M. Kloxin, A.M. Kasko, C.N. Salinas, K.S. Anseth, Science 324 (5923) (2009) 59–63, http://dx.doi.org/10.1126/science.1169494.
[4] R. DeVolder, H.-J. Kong, Wiley Interdiscip. Rev. Syst. Biol. Med. 4 (4) (2012) 351–365, http://dx.doi.org/10.1002/wsbm.1174.
[5] P. Carmeliet, R.K. Jain, Nature 407 (6801) (2000) 249–257, http://dx.doi.org/10.1038/35025220.
[6] M. Belting, M.I. Dorrell, S. Sandgren, E. Aguilar, J. Ahamed, A. Dorfleutner, P. Carmeliet, B.M. Mueller, M. Friedlander, W. Ruf, Nat. Med. 10 (5) (2004) 502–509, http://dx.doi.org/10.1038/nm1037.
[7] Y. Dor, V. Djonov, E. Keshet, Trends Cell Biol. 13 (3) (2003) 131–136, http://dx.doi.org/10.1016/s0962-8924(03)00022-9.
[8] P. Carmeliet, Nature 438 (7070) (2005) 932–936, http://dx.doi.org/10.1038/nature04478.
[9] L. Coultas, K. Chawengsaksophak, J. Rossant, Nature 438 (7070) (2005) 937–945, http://dx.doi.org/10.1038/nature04479.
[10] S. Van Vlierberghe, P. Dubruel, E. Schacht, Biomacromolecules 12 (5) (2011) 1387–1408, http://dx.doi.org/10.1021/bm200083n.
[11] N. Yonet-Tanyeri, M.H. Rich, M. Lee, M.H. Lai, J.H. Jeong, R.J. DeVolder, H. Kong, Biomaterials 34 (33) (2013) 8416–8423, http://dx.doi.org/10.1016/j.biomaterials.2013.07.026.
[12] J.L. Drury, D.J. Mooney, Biomaterials 24 (24) (2003) 4337–4351, http://dx.doi.org/10.1016/s0142-9612(03)00340-5.
[13] N.A. Peppas, J.Z. Hilt, A. Khademhosseini, R. Langer, Adv. Mater. 18 (11) (2006) 1345–1360, http://dx.doi.org/10.1002/adma.200501612.
[14] M.R. Guilherme, A.V. Reis, A.T. Paulino, T.A. Moia, L.H.C. Mattoso, E.B. Tambourgi, J. Appl. Polym. Sci. (2010), http://dx.doi.org/10.1002/app.32123 (n/a–n/a.).
[15] U. Gbureck, T. Hölzel, C.J. Doillon, F.A. Müller, J.E. Barralet, Adv. Mater. 19 (6) (2007) 795–800, http://dx.doi.org/10.1002/adma.200601370.
[16] I. Barkefors, S. Thorslund, F. Nikolajeff, J. Kreuger, Lab Chip 9 (4) (2009) 529–535, http://dx.doi.org/10.1039/b814691h.
[17] J.H. Jeong, V. Chan, C. Cha, P. Zorlutuna, C. Dyck, K.J. Hsia, R. Bashir, H. Kong, Adv. Mater. 24 (1) (2012) 58–63, http://dx.doi.org/10.1002/adma.201103207.
[18] E.A. Silva, D.J. Mooney, Biomaterials 31 (6) (2010) 1235–1241, http://dx.doi.org/10.1016/j.biomaterials.2009.10.052.
[19] G.E. Davis, D.R. Senger, Circ. Res. 97 (11) (2005) 1093–1107, http://dx.doi.org/10.1161/01.RES.0000191547.64391.e3.
[20] G. Bergers, L.E. Benjamin, Nat. Rev. Cancer 3 (6) (2003) 401–410, http://dx.doi.org/10.1038/nrc1093.
[21] A.V. Benest, H.G. Augustin, Nat. Med. 15 (6) (2009) 608–610, http://dx.doi.org/10.1038/nm0609-608.
[22] P. Carmeliet, R.K. Jain, Nat. Rev. Drug Discov. 10 (6) (2011) 417–427, http://dx.doi.org/10.1038/nrd3455.
[23] L.J. Millet, M.B. Collens, G.L.W. Perry, R. Bashir, Integr. Biol. 3 (12) (2011) 1167, http://dx.doi.org/10.1039/c1ib00054c.
[24] K. Baek, J.H. Jeong, A. Shkumatov, R. Bashir, H. Kong, Adv. Mater. 25 (39) (2013) 5568–5573, http://dx.doi.org/10.1002/adma.201300951.
[25] J. Dong, B.Z. Chowdhry, S.A. Leharne, Colloids Surf. A Physicochem. Eng. Asp. 212 (1) (2003) 9–17, http://dx.doi.org/10.1016/s0927-7757(02)00295-9.
[26] B.K. Lee, Y.H. Yun, J.S. Choi, Y.C. Choi, J.D. Kim, Y.W. Cho, Int. J. Pharm. 427 (2) (2012) 305–310, http://dx.doi.org/10.1016/j.ijpharm.2012.02.011.
[27] A.S. Chung, N. Ferrara, Annu. Rev. Cell Dev. Biol. 27 (1) (2011) 563–584, http://dx.doi.org/10.1146/annurev-cellbio-092910-154002.
[28] A.H. Zisch, M.P. Lutolf, J.A. Hubbell, Cardiovasc. Pathol. 12 (6) (2003) 295–310, http://dx.doi.org/10.1016/s1054-8807(03)00089-9.
[29] H.C. Han, J. Vasc. Res. 49 (3) (2012) 185–197, http://dx.doi.org/10.1159/000335123.
[30] R. Pasqualini, W. Arap, D.M. McDonald, Trends Mol. Med. 8 (12) (2002) 563–571, http://dx.doi.org/10.1016/s1471-4914(02)02429-2.
[31] A. Hoeben, B. Landuyt, M.S. Highley, H. Wildiers, A.T. Van Oosterom, E.A. De Bruijn, Pharmacol. Rev. 56 (4) (2004) 549–580, http://dx.doi.org/10.1124/pr.56.4.3.

[32] S.D. Croll, R.M. Ransohoff, N. Cai, Q. Zhang, F.J. Martin, T. Wei, L.J. Kasselman, J. Kintner, A.J. Murphy, G.D. Yancopoulos, S.J. Wiegand, Exp. Neurol. 187 (2) (2004) 388–402, http://dx.doi.org/10.1016/j.expneurol.2004.02.010.
[33] G.D. Yancopoulos, S. Davis, N.W. Gale, J.S. Rudge, S.J. Wiegand, J. Holash, Nature 407 (6801) (2000) 242–248, http://dx.doi.org/10.1038/35025215.
[34] N. Ferrara, H.P. Gerber, J. LeCouter, Nat. Med. 9 (6) (2003) 669–676, http://dx.doi.org/10.1038/nm0603-669.
[35] E.A. Silva, D.J. Mooney, 64 (2004) 181–205, http://dx.doi.org/10.1016/s0070-2153(04)64008-7.
[36] P. Carmeliet, E.M. Conway, Nat. Biotechnol. 19 (11) (2001) 1019–1020, http://dx.doi.org/10.1038/nbt1101-1019.
[37] M. Simons, R.O. Bonow, N.A. Chronos, D.J. Cohen, F.J. Giordano, H.K. Hammond, R.J. Laham, W. Li, M. Pike, F.W. Sellke, T.J. Stegmann, J.E. Udelson, T.K. Rosengart, Circulation 102 (11) (2000) e73–e86, http://dx.doi.org/10.1161/01.CIR.102.11.e73.
[38] K.Y. Lee, M.C. Peters, K.W. Anderson, D.J. Mooney, Nature 408 (6815) (2000) 998–1000, http://dx.doi.org/10.1038/35050141.
[39] E.A. Silva, D.J. Mooney, J. Thromb. Haemost. 5 (3) (2007) 590–598, http://dx.doi.org/10.1111/j.1538-7836.2007.02386.x.
[40] Y. Lei, H. Haider, J. Shujia, E.S. Sim, Basic Res. Cardiol. 99 (2) (2004) 121–132, http://dx.doi.org/10.1007/s00395-004-0447-x.
[41] G.V. Silva, S. Litovsky, J.A. Assad, A.L. Sousa, B.J. Martin, D. Vela, S.C. Coulter, J. Lin, J. Ober, W.K. Vaughn, R.V. Branco, E.M. Oliveira, R. He, Y.J. Geng, J.T. Willerson, E.C. Perin, Circulation 111 (2) (2005) 150–156, http://dx.doi.org/10.1161/01.CIR.0000151812.86142.45.
[42] S. Takeshita, L.P. Zheng, E. Brogi, M. Kearney, L.-Q. Pu, S. Bunting, N. Ferrara, J.F. Symes, J.M. Isner, J. Clin. Invest. 93 (1994) 662–670.